Journal of Applied Polymer Science

Protective Properties of PPy-Au Nanocomposite Coatings Prepared by Sonoelectrochemisty and Optimized by the Taguchi Method

Habib Ashassi-Sorkhabi, Robabeh Bagheri, Babak Rezaei-Moghadam
Department of Physical Chemistry, Electrochemistry Research Laboratory, Faculty of Chemistry, University of Tabriz, Tabriz, Iran
Correspondence to: H. Ashassi-Sorkhabi (E-mail: ashassi@tabrizu.ac.ir)

ABSTRACT: The polypyrrole (PPy) and polypyrrole-Au (PPy-Au) nanocomposite films have been sonoelectrochemically synthesized on St-12 steel electrodes using the galvanostatic technique. Experimental design according to the Taguchi method has been applied to optimize the factors on the synthesis of PPy-Au nanocomposite coating. Three factors were used to design an orthogonal array L9: Synthesis time (t), Current density (I), and Concentration of $HAuCl_4$ (C). The synthesized Au nanoparticles during polymerization were characterized by Ultraviolet–visible (UV-visible) spectroscopy. Characterization of the surfaces was done by scanning electron microscope (SEM), energy dispersive X-ray spectrum (EDX), and atomic force microscope (AFM). The scanning electron microscopy (SEM) image of PPy shows a smooth surface while PPy-Au nanocomposite film has a compact morphology. Moreover, energy dispersive X-ray spectrum (EDX) is evidence for the incorporation of Au nanoparticles. The corrosion protection of coatings was investigated by open circuit potential (OCP) time trends, potentiodynamic polarization technique, and electrochemical impedance spectroscopy (EIS) in a NaCl 3.5% solution. © 2014 Wiley Periodicals, Inc. J. Appl. Polym. Sci. **2014**, *131*, 41087.

KEYWORDS: conducting polymers; coatings; electrochemistry; nanoparticles; nanowires and nanocrystals

Received 25 January 2014; accepted 31 May 2014
DOI: 10.1002/app.41087

INTRODUCTION

Intrinsically conducting polymers such as polyaniline (PANI), polythiophene, or polypyrrole (PPy) are used in scientific, industrial studies, and in various applications such as rechargeable batteries,[1,2] sensors,[3,4] and corrosion protection.[5–11] The use of polyaniline[12–14] and polypyrrole[15–20] as corrosion protection coating of metals has been investigated in many articles. However, the porosity and ion exchange ability of conducting polymer coatings might be disadvantageous for corrosion protection performance. The charges stored in the polymer layer can be irreversibly consumed during the system's redox reactions, and the ability of the protection with polymer coatings may be lost with time. Therefore, nanostructure materials such as nanocomposites have been synthesized due to their specific properties.

To date, many papers have been published dealing with the chemical[21,22] and electrochemical[23–25] synthesis of nanocomposites and their corrosion protection properties. Electrochemically synthesis methods are favored because of the direct synthesis of a polymer on the metal surface without any organic additives[26] and capability of preparing smaller and size-controllable metal particles by adjusting the applied potential or the current density.[27]

Also, Jing et al. showed that the ultrasonic irradiation has been applied to improve the mechanical properties of the coatings. The authors attributed these observations to the high mass transport of monomers and perhaps enhancement of the adhesion of polymer to the metal surface.[28,29]

According to literature the Polypyrrol coatings were synthesized by chemical,[30] electrochemical,[31] and sonoelectrochemical methods at high frequency[32] and in our previous work at low frequency.[33] On the other hand, Polypyrrole–Au nanocomposites were synthesized by chemical,[34] sonochemical,[35] and electrochemical[36,37] methods. However, we could not find any reports about the application of sonoelectrochemical method for synthesis of PPy-Au on St-12 steel. In this study, we propose a new process for direct in situ sonoelectrosynthesis of PPy-Au nanocomposite. Our interest is the galvanostatic preparation of nanocomposite under irradiation of ultrasound and optimizing the synthesis conditions using Taguchi method.

EXPERIMENTAL

Materials

Pyrrole (97%) and oxalic acid (99%) were purchased from Merck (Germany). Dodecylbenzene sulfonic acid (DBSA) as acid dopant was supplied by Fluka. Chloroauric acid, $HAuCl_4 \cdot H_2O$, (48% Au, Germany) was used as Au ions. Pyrrole was purified by distillation just before use and other chemicals were used without any further purification. All the aqueous solutions were prepared using distilled water. The St-12 steel

Table I. The Main Content of the St-12 Steel

Fe 99.6	C 0.046	Mn 0.215	P 0.006	S 0.006	Cr 0.013	Mo 0.002	Ni 0.038
Al 0.040	Co 0.008	Cu 0.022	Nb 0.002	Ti 0.003	V 0.003	W 0.007	Sn 0.010
Mg 0.003	Zn 0.015	Pb 0.001	As 0.001	Zr 0.001	Ce 0.001	Sb 0.001	Ta 0.002

sheet (1×1 cm^2) was used as a working electrode and its chemical content is given in Table I.

Instruments

The UV−visible spectrophotometer (HACH DR 5000) was used to characterize the synthesized gold nanoparticles formed during sonoelectrodeposition in the bath solution. An Autolab Potentiostat/Galvanostat (Netherland Instruments) was employed for the synthesis and corrosion measurements of the coatings. Potentiodynamic polarization and electrochemical impedance spectroscopy tests carried out at 298 K using GPES and FRA software, respectively.

The results were analyzed by Zview® (II) software and an appropriate equivalent electrochemical circuit was proposed. The SEM micrographs were prepared using scanning electron microscope (KYKY-EM3200 model) and surface characterization of coatings was performed by atomic force microscopy, AFM (Model Nanosurf Mobiles Company Nanosurf, Switzerland). Dr. Hielscher S400UP ultrasound generator with a titanium horn 22H was used as ultrasound wave source for sonoelectropolymerization. Experiments conducted under ultrasound irradiation were performed at a constant ultrasonic frequency of 24 kHz in a 150 mL cell. The polymerization was performed in a glass cell that located in the ultrasonic box.

Experimental Design

An experimental design, based on the Taguchi method, was employed to determine the optimum condition with respect to the synthesis time, applied current density, and the concentration of $HAuCl_4$ to achieve the minimum average size of nanoparticles. The Minitab software was used, and the average of responses at each level for various factors was plotted. For the case of minimization of size of nanoparticles, the wavelength of UV-spectra of AuNPs intended to be minimized.

Sonoelectrodeposition of Nanocomposite Coatings

In this study, electrochemical synthesis was carried out under galvanostatic conditions at room temperature. Preparation of PPy-Au nanocomposite was performed in a beaker containing a Pt sheet as counter, St-12 steel as a working and Saturated Calomel Electrode (SCE) as a reference electrode. The aqueous electrolyte solution consists of oxalic acid (0.1*M*), pyrrole monomer (0.1*M*), DBSA (100 ppm), and optimum concentration (10 ppm) of $HAuCl_4$ which is obtained by Taguchi design. The solution was prepared by dissolving appropriate volume of distilled pyrrole in oxalic acid and DBSA. Then chloroauric acid (3.5, 7, and 10 ppm) was added in the solution.

In order to direct *in situ* preparation of PPy-Au nanocomposite coatings, electropolymerization was performed using a constant current density in the presence of the sono-irradiation power. The tip of the horn that was attached to the power supply of the sonication device was inserted into the solution. Prior to each experiment, a working electrode was mechanically polished by a sequence of emery papers of various increasing grades (400–2500 grit), rinsed with distilled water, and then degreased. A schematic diagram of the sonoelectrorchemical synthesis set-up of coatings is shown in Figure 1.

The Taguchi method was used to determine the influence of the different parameters such as current density, synthesis time, and concentration of $HAuCl_4$ on nanoparticles preparation. The UV−visible spectrophotometer was used to characterize the AuNPs during the synthesis.

Electrochemical Corrosion Study

The open circuit potential (OCP), electrochemical impedance spectroscopy, (EIS), and Tafel polarization measurements were used to investigate the corrosion performance of the synthesized coatings. The synthesized coatings were immersed in 3.5% NaCl at open circuit condition for 10 minutes in order to reach a constant equilibrium potential. The Nyquist plots were recorded at instantaneous open circuit potential values in a frequency range of 10 kHz to 10 mHz.

RESULTS AND DISCUSSION

Sonoelectrochemical Synthesis

In situ sonoelectrochemical synthesis of PPy together with Au nanoparticles carried out in 0.1*M* oxalic acid solution containing pyrrole 0.1*M* and $HAuCl_4$. The galvanostatic technique and ultrasonic irradiation were applied to oxidation of pyrrole monomer and reduction of $HAuCl_4$ simultaneously. It can be said that the PPy acts as a stabilizer for synthesized Au nanoparticles and ultimately, the PPy-Au nanocomposite films were precipitated on a St-12 steel electrode. To characterize the AuNPs, the UV–visible spectrum from treated solution was recorded (Figure 2). It is clear that in the beginning of the

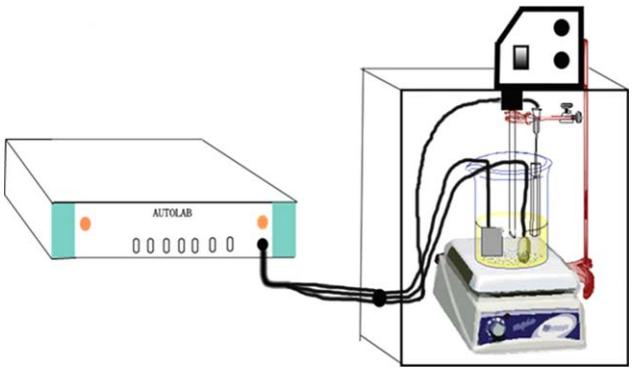

Figure 1. Experimental set up for sonoelectrochemical synthesis. [Color figure can be viewed in the online issue, which is available at wileyonlinelibrary.com.]

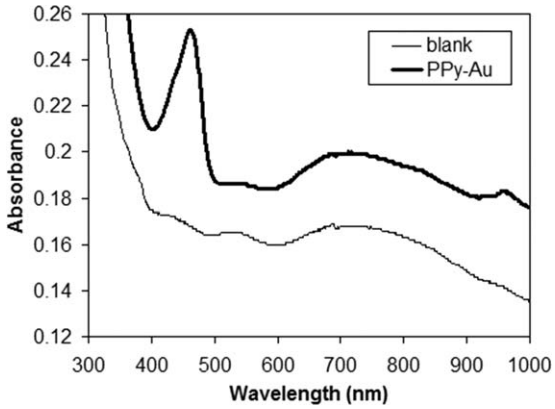

Figure 2. UV-Vis spectra of solution before polymerization containing: pyrrole monomer, Au salt and DBSA (blank) and after synthesis of PPy-Au nanocomposite.

experiment, the peak of the curve is not seen while the sharp peak is observed after 10 min. The typical peak at around 450 nm reveals the formation of Au nanoparticles.[34,38] Figure 3 shows the potential versus time curves (galvanostatic measurement) for sonoelectrodeposition of PPy and PPy-Au nanocomposite coatings on St-12 steel. It is obvious that both plots show the same behavior and consist of three regions: the induction time is attributed to an active dissolution of iron at negative potential, precipitation of Fe (II) oxalate, and electropolymerization of PPy (or PPy-Au nanocomposite).

Taguchi Design of Experiment

Design of Orthogonal Array and ANOVA Analysis. In the Taguchi method, orthogonal arrays and analysis of variance (ANOVA) are used as tools of analysis. This method can minimize the number of experiments using a statistical design of experiments.[39–42]

In this work, three factors (synthesis time, applied current density, and concentration of $HAuCl_4$) with three levels were used to design the L9 orthogonal array. Design factors,

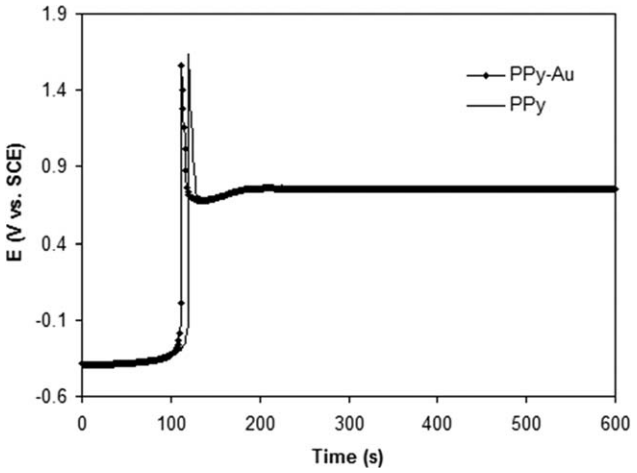

Figure 3. Potential time curves for the sonoelectrodeposition of PPy and PPy-Au on st-12 steel from aqueous electrolyte (0.1*M* pyrrole, 0.1*M* $H_2C_2O_4$) at a current density of 4 mA cm^{-2}.

Table II. Design Factors, Response, and Their Levels

		Factor			Response
Levels		I (mA/cm^2)	Time (s)	C (ppm)	λ_{max} (nm)
1	111	3	600	3.5	455
2	122	3	1,200	7	457
3	133	3	1,800	10	462
4	212	4	600	7	450
5	223	4	1,200	10	454
6	231	4	1,800	3.5	460
7	313	5	600	10	454
8	321	5	1,200	3.5	457
9	332	5	1,800	7	460

response, and their levels are shown in Table II. The parameters were optimized with the objective of minimizing the wavelength (λ_{max}).

The average λ_{max} values at different levels are summarized in Table III. Rank values based on Delta statistics, which compare the relative magnitude of effects, show that the time of synthesis is the most effective parameter. In addition, the analysis of variance (ANOVA) results was listed in Table IV. The low P-value of model ($P < 0.05$) indicates that the Taguchi model is statistically significant.

Main Effects. The corresponding main-effect plots of three parameters are shown in Figure 4. It can be seen from Figure 4(a) that the average λ_{max} values drop to the bottom of the curve as the applied current density increased from 3 to 4 mA/cm^2, and in Figure 4(b) the average λ_{max} values increased by increasing the time of synthesis. The concentration of $HAuCl_4$ has a negligible contribution on the average λ_{max} values. It is clear that a parameter for which the line has the highest inclination will have the most significant effect.

Determination of the Optimal Conditions Using Taguchi Method. Since the size of synthesized nanoparticles intended to be minimized, the mean square deviation (MSD) for lower-the-better characteristics of responses was selected, which can be calculated using the following equation[43]:

$$\mathrm{MSD} = \frac{1}{n}\sum_{i=1}^{n}\frac{1}{y_i^2} \quad (1)$$

where y is the observed data, and n is the number of observations.

Table III. Response Table for Means

Level	I (mA cm^{-2})	Time (s)	C (ppm)
1	458.0	453.0	457.3
2	454.7	456.0	455.7
3	457.0	460.7	456.7
Delta	3.3	7.7	1.7
Rank	2	1	3

Table IV. ANOVA for the Fit of the Experimental Data to Taguchi Model

Source of variation	Degree of freedom	Sum of squares	*F*-value	*P*-Value
Current density	2	17.556	19.75	0.048
Time	2	89.556	100.75	0.010
Concentration	2	4.222	4.75	0.174
Error	2	0.889		
Total	8	112.222		

$R^2 = 99.21\%$, $R^2(\text{adj}) = 96.83\%$.

By selecting the lowest value of MSD result for each factor, the optimal level can be determined. On this basis, the optimum combination of levels in terms of minimizing the particle size is 4 mA cm^{-2} for current density, 600 s for synthesis time, and 7 ppm for the concentration of $HAuCl_4$. The confirmation test was performed, and the correlation between predicted and actual average λ_{max} values is depicted in Figure 5. Having *R* square being equal to 99.21% confirms that the fitted model to the results is acceptable.

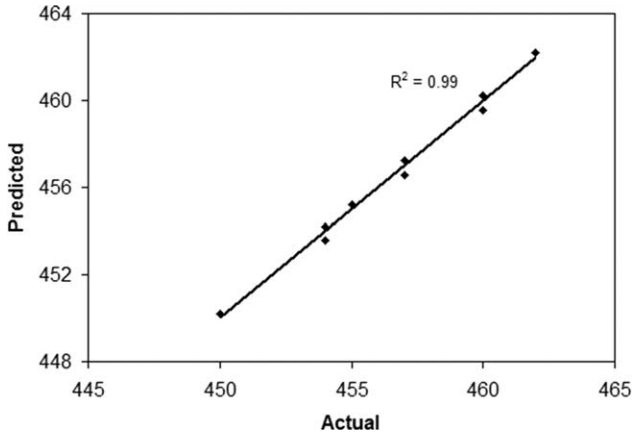

Figure 5. Correlation between predicted and actual results of the average λ_{max} values according to the L9 OA designed factors listed in Table II.

Characterization of Coatings

The SEM images of PPy and PPy-Au nanocomposite coatings, synthesized by sonoelectrochemical method, were shown in Figure 6. The coating thickness examined by SEM was about 2.4 μm. It is clear that the PPy film (a) exhibited a better homogeneity at the surface with respect to the PPy-Au coating (b). The expanded view of the PPy-Au nanocomposite coating with magnification of 15 kx is shown in Figure 6(c). Comparing these figures show that the incorporation of Au nanoparticles with PPy coating caused a great change on the surface morphology. It can be deduced that PPy-Au nanocomposite coating exhibited more compact surface in comparison with PPy coating. Also, the codeposited nanoparticles act as barriers in growth of corrosion paths and stop the columnar growth. These paths increase the tortuosity of diffusion path-way of corrosion specimen and caused to high corrosion resistance in comparison with pure PPy coatings.

The corresponding peak of Au in EDX analyze results of PPy-Au coatings is evidence for the incorporation of Au nanoparticles [Figure 6(d)]. The composition of PPy-Au nanocomposite coating is (at. %): C = 63.51, N = 20.32, O = 14.92, and Au = 1.25.

Figure 7 shows the AFM images of PPy and PPy-Au coatings deposited on St-12 steel. It can be seen that the roughness of PPy-Au nanocomposite coating is higher than the roughness of PPy and is more compact compared with the PPy, which confirmed the SEM results.

Corrosion Studies

Open Circuit Potential (O.C.P). The corrosion resistance of the PPy and PPy-Au nanocomposite films was studied by immersion

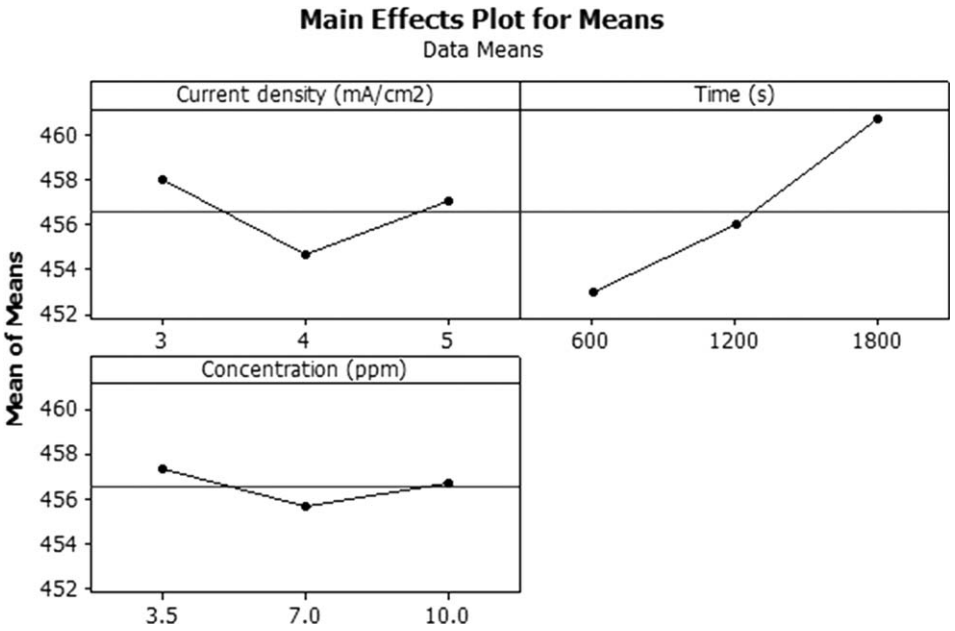

Figure 4. Effects of (a) current density, (b) synthesis time, and (c) $HAuCl_4$ concentration on average λ_{max} values.

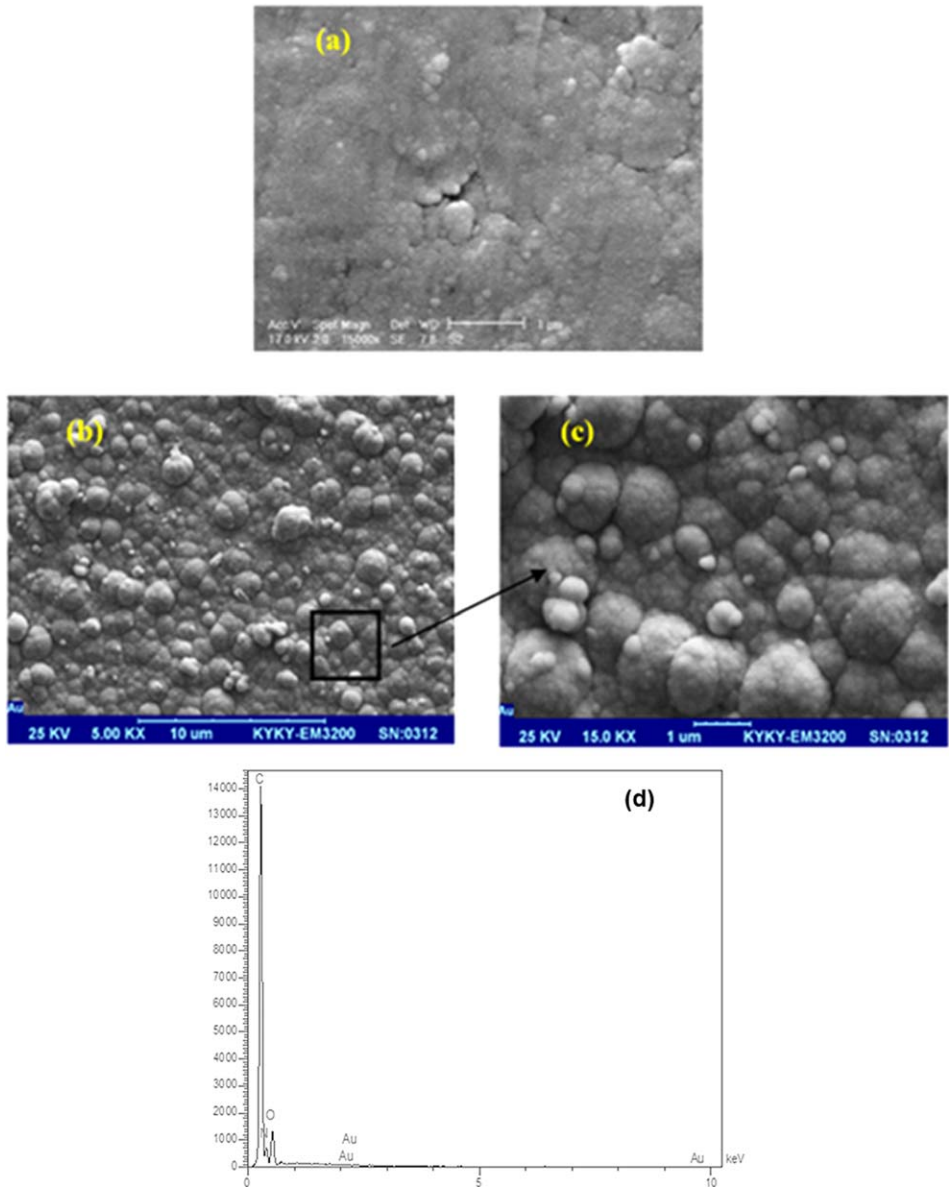

Figure 6. SEM images of: (a) PPy and (b) PPy-Au coatings: ×5000, (c) expanded view of the PPy-Au nanocomposite coating: 15 kx, and (d) Energy dispersive X-ray spectrum of PPy-Au nanocomposite coatings. Composition (at. %): C = 63.51, N = 20.32, O = 14.92, and Au = 1.25. [Color figure can be viewed in the online issue, which is available at wileyonlinelibrary.com.]

of the samples in 3.5% NaCl solution. The open circuit potential (E_{OCP}) of the electrode systems was measured versus time and plotted on the graph as shown in Figure 8. The initial potential of the nanocomposite was more positive than that for PPy film. After 10 min of immersion, the corrosion potential of PPy-Au nanocomposite and PPy coatings were (−10 mV) and (−250 mV) respectively. High E_{OCP} value of nanocomposite compared with that of PPy coatings clearly indicates the high corrosion resistance provided by these coatings.[44] It can be concluded that the more barrier effect of nanocomposite coating suppresses the active dissolution of steel, facilitating the potential to be shifted in the passive region.

Potentiodynamic Studies. The polarization curves for the St-12 steel and coatings are shown in Figure 9. The values of the electrochemical corrosion parameters such as corrosion potential (E_{corr}), cathodic (b_c), and anodic (b_a) Tafel slope, and corrosion current density (I_{corr}) that evaluated from Figure 9 are presented in Table V. The corrosion current density, I_{corr}, is a parameter to characterize the corrosion rate. It is obtained that the I_{corr} for the PPy coatings is considerably higher than that for PPy-Au nanocomposite coatings. This may be attributed to the fact that the synthesis of nanoparticles during the polymerization of PPy made it a dense nanocomposite film. The presence of Au nanoparticles provides new and appropriate sites for polymerization, so that the sites' number in this case is higher than the case of polymerization in the absence of nanoparticles. Generally, it was observed that the PPy-Au nanocomposites coatings form compact films on a St-12 steel surfaces with low

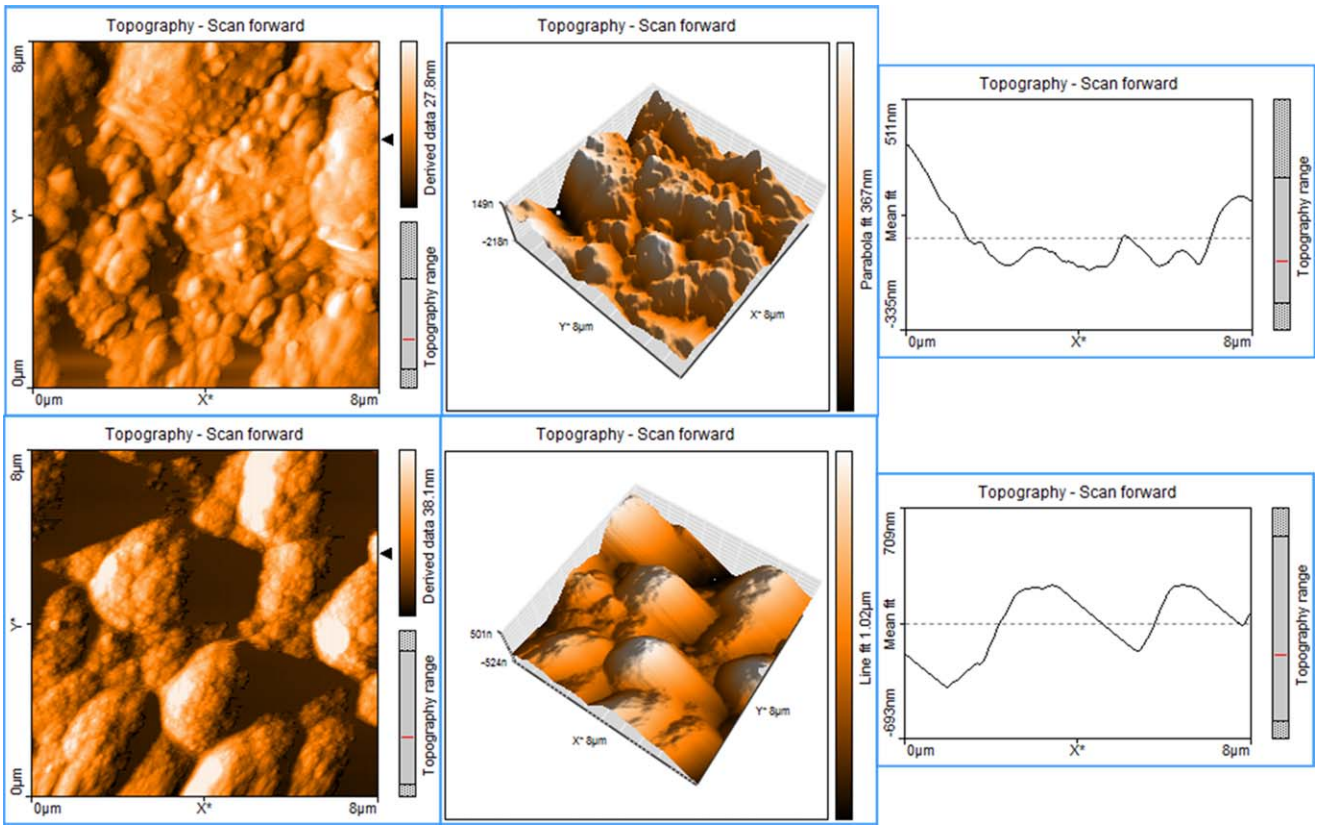

Figure 7. Topographic AFM image of (a) PPy and (b) PPy/Au coatings on St-12 steel. [Color figure can be viewed in the online issue, which is available at wileyonlinelibrary.com.]

porosity. To calculate the porosity of these coatings, we have used the following relationship:[45]

$$\%P = \frac{R_P^0}{R_P} \times 10^{\left(\frac{-\Delta E_{corr}}{b_a^0}\right)} \times 100 \quad (2)$$

where P is the total porosity, R_p^0 and R_p are the polarization resistance of bare and coated steel, respectively, ΔE_{corr} is the difference of the corrosion potential between the coating and the substrate, and b_a^0 is the anodic Tafel slope of the substrate. Using the above equation and the electrochemical data gives a porosity of 0.01% for PPy-Au nanocomposite that is very low with respect to PPy coatings having a porosity of 2.86%. It can be found that, the lower the calculated porosity, the higher is the protective efficiency.

Electrochemical Impedance Spectroscopy Studies. The nyquist plots for St-12 steel, PPy, and PPy-Au coatings in 3.5% NaCl solution are shown in Figure 10. The interpretation of impedance spectra was performed after numerical fitting using the

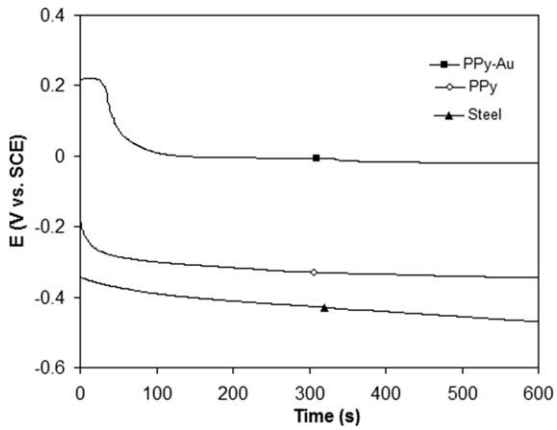

Figure 8. The variation of E_{OCP} values with increasing exposure time in 3.5% NaCl solution for St-12 steel, PPy, and PPy-Au.

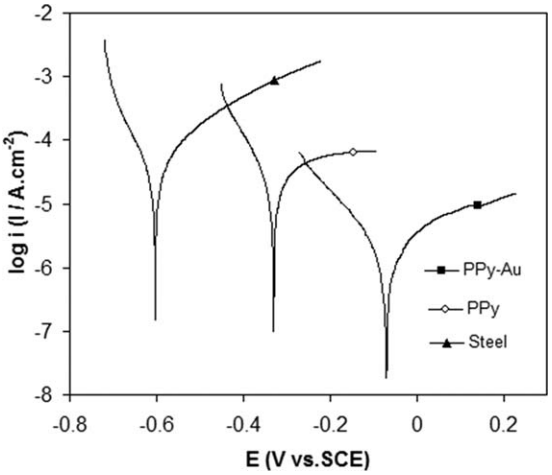

Figure 9. Tafel plot of samples with scan rate of 0.5 mV s^{-1} for St-12 steel, PPy, and PPy-Au nanocomposite coatings.

Table V. Corrosion Parameters for Coatings on St-12 Steel in 3.5% NaCl Solution

Sample	E_{corr} (V/SCE)	i_{corr} (μA/cm^2)	b_a (mV/decade)	$-b_c$ (mV/decade)	R_p (Ω cm^2)	*C.R* (mm/year)	%*P*
St-12 steel	−602	49.13	215.05	75.12	514	0.57	–
PPy	−338.00	26.97	414	79	1,068	0.31	2.86
PPy-Au	−67.79	1.82	268	105	17,978	0.02	0.010

suitable equivalent circuits presented in Figure 11 and the rendered data shown in Table VI.

The most common equivalent circuit that used to fit the corrosion data of bare St-12 steel in NaCl 3.5% solution was the Randles circuit as Figure 11(a). Where R_s is the solution resistance, R_{corr} is the corrosion resistance and the CPE is constant phase element for the double layer capacitance. Considering the Nyquist plot of PPy-Au nanocomposite coating, it appears that there are two semicircles, including two times constant while the plot for PPy coating also includes two semicircles as PPy-Au nanocomposite coating but these semicircles followed by a straight line at low frequencies [Figure 11(b,c)]. The linear part is characteristic of the lower frequency range and represents the diffusion controlled electrode process, which gives rise to a Warburg impedance element in the electrical circuit. A Warburg element occurs when charge carrier diffuses through a material. Lower frequencies correspond to diffusion deeper into the material. W-R, W-T, and W-P are three characters of the finite length Warburg element. The W-R and W-T value represents the Warburg resistance and Warburg coefficient, respectively and W-P is exponent, which set in 0.5.

As mentioned above, two capacitive depressed semi-circles are present for the PPy and PPy-Au coated samples in the Nyquist diagrams. One of them at high frequencies is attributed to the electrical properties of the film (R_{coat}) and the other to processes occurring under the coatings (R_{corr}). The constant phase element for coating is indicated by CPE-1 and complex impedance of a constant phase element (CPE) is defined as below:

$$Z_{CPE} = Q^{-1}(j\omega)^{-n} \quad (3)$$

where Z_{CPE} is the impedance of the constant phase elements, ω is the angular frequency of alternating current voltage, Q and n are the frequency independent parameters.[45–47] The constant phase elements CPE-1 and CPE-2 are electrical double layer pseudo-capacitances of the coat/electrolyte and corroding metal/coat electrochemical interfaces, respectively.

Comparison between R_{corr} value of PPy and PPy-Au nanocomposite coating on St-12 steel predicts that the PPy-Au coating has significantly higher corrosion protection properties.

The excellent anticorrosion protection is attributed to the size of nanoparticles, which has the small size and large aspect ratio. For the small particles, free space between the particles and polymer is far lesser than that of larger particles. Thus electrolyte is harder to penetrate through the pores in coating film with addition of nanoparticles. In addition due to longer diffusion path in the nanocomposite film, the water and ions need more time to arrive at the substrate. Generally, it was observed that the PPy-Au nanocomposite coatings form compact films on the St-12 steel surfaces with low porosity. Therefore, in the

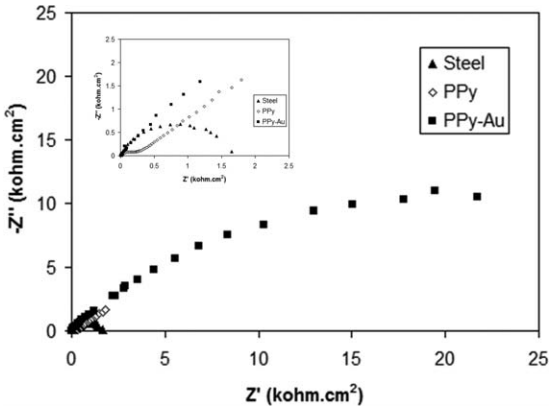

Figure 10. The Nyquist plots for St-12 steel, PPy, and PPy-Au coatings in 3.5% NaCl solution.

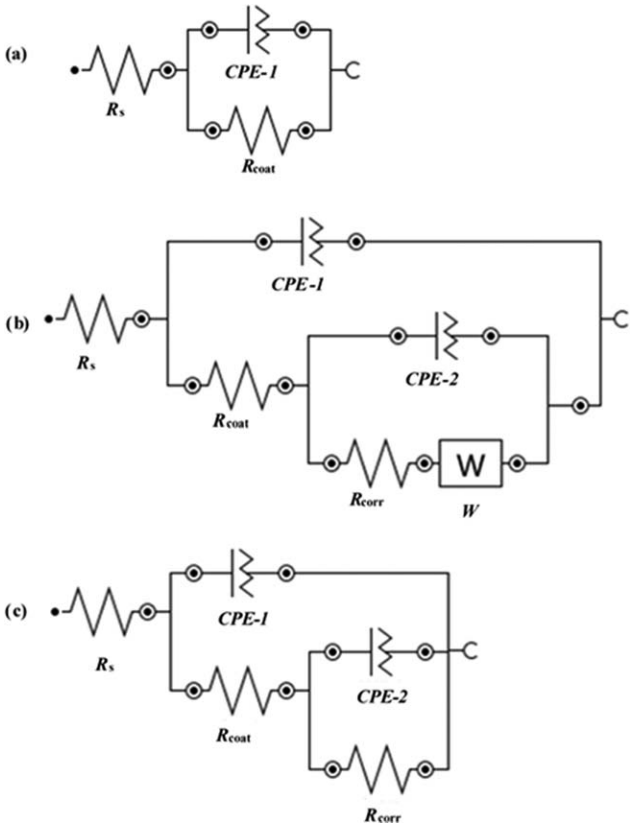

Figure 11. Electrical circuit model for (a) St-12 steel, (b) PPy, and (c) PPy-Au nanocomposite coatings behavior.

Table VI. Corrosion Resistance Behavior of St-12 Steel Electrode Coated with PPy and PPy–Au in 3.5% NaCl Solution Evaluated by Electrochemical Impedance Spectroscopy

		CPE-1			CPE-2					
Sample	R_s (Ω cm^2)	$Q_1 \times 10^{-5}$ (Ω^{-1} cm^{-2}s^n)	n_1	R_{coat} (Ω cm^2)	$Q_2 \times 10^{-5}$ (Ω^{-1} cm^{-2} s^n)	n_2	R_{corr} (Ω cm^2)	*W-R*	*W-T*	*W-p*
St-12 steel	7.2	–	–	–	63.1	0.75	1962	–	–	-
PPy	10	0.90	0.82	176	69.00	0.50	243	14710	213.2	0.5
PPy-Au	7	6.32	0.72	4036	1.46	0.56	35408	–	–	–

case of nanocomposite coatings, the Au nanoparticles probably block effectively the pores existing in the PPy coatings.

The stability of the coating after immersion in the NaCl 3.5% solution was investigated by electrochemical methods. It is found that the corrosion rate of PPy-Au nanocomposite coating obtained by Tafel polarization is 0.02 mm/year which is very low (about 15 times lower) in comparison with PPy coating (0.31 mm/year).

CONCLUSIONS

In this study, PPy and PPy-Au nanocomposite coatings were electropolymerized on a St-12 steel substrate in a 0.1*M* oxalic acid aqueous solution containing 0.1M pyrrole and desired concentration of gold compound under ultrasonic irradiation. The sonoelectrosynthesis of coatings in proposed bath has some advantages, such as low cost, simplicity of the method and the absence of organic solvents. Galvanostatic method was successfully employed for the preparation of Au nanoparticles in the presence of PPy. It is found that the synthesis time and applied current density play an important role in the size of synthesized nanoparticles. Taguchi orthogonal array was employed to optimize the current density and other parameters to reach the minimum average size of nanoparticles. The optimized synthesis parameters are current density of 4 mA cm^{-2}, synthesis time of 600 s and 7 ppm $HAuCl_4$ concentration. The SEM imaging, EDX analysis and AFM images were used to characterize the surface properties of coatings. These investigations showed that PPy-Au nanocomposite films are more compact compared to the PPy films. The obtained results for the corrosion behavior of the coatings indicate a significant anticorrosion performance of PPy-Au nanocomposite deposited on the St-12 steel surface.

This work has been performed under the auspices of the University of Tabriz. Authors are grateful for financial support from Research Office of the University of Tabriz. Authors are also cordially grateful for Iran Nanotechnology Initiative Council financial supports.

REFERENCES

1. Balis, N.; Dracopoulos, V.; Antoniadou, M.; Lianos, P. *Electrochim. Acta* **2012**, *70*, 338.
2. Lakard, B.; Ploux, L.; Anselme, K.; Lallemand, F.; Lakard, S.; Nardin, M.; Hihn, J. Y. *Bioelectrochemistry* **2009**, *75*, 148.
3. Zhang, M.; Yamaguchi, A.; Morita, K.; Teramae, N. *Electrochem. Commun.* **2008**, *10*, 1090.
4. Li, J.; Xieand, H.; Li, Y. *J. Solid State Electrochem.* **2012**, *16*, 795.
5. Jeon, H.; Park, J.; Shon, M. *J. Indust. Eng. Chem.* **2013**, *19*, 849.
6. Le, H. N. T.; Garcia, B.; Deslouis, C.; Xuan, Q. L. *Electrochim. Acta* **2001**, *46*, 4259.
7. Ocon, P.; Cristobal, A. B.; Herrasti, P.; Fatas, E. *Corros. Sci.* **2005**, *47*, 649.
8. Ohtsuka, T. *Int. J. Corr.* **2012**, *2012*, 1.
9. Wei, H.; Ding, D.; Weiand, S.; Guo, Z. *J. Mater. Chem. A.* **2013**, *1*, 10805.
10. Yu, Y.-H.; Lin, Y.-Y.; Lin, C.-H.; Chana, C.-C.; Huang, Y.-C. *Polym. Chem.* **2014**, *5*, 535.
11. Shabani-Nooshabad, M.; Ghoreishi, S. M.; Behpour, M. *Corrosion Sci.* **2011**, *53*, 3035.
12. Hoang, H. V.; Holze, R. *Chem. Mater.* **2006**, *18*, 1976.
13. Ganash, A. A.; Al-Nowaiser, F. M.; Al-Thabaiti, S. A.; Hermas, A. A. *J. Solid State Electrochem.* **2013**, *17*, 849.
14. Senarathna, K. G. C.; Mantilaka, M. M. M. G. P. G.; Peiris, T. A. N.; Pitawala, H. M. T. G. A.; Karunaratne, D. G. G. P.; Rajapakse, R. M. G. *Electrochim. Acta* **2014**, *117*, 460.
15. Ferreira, C. A.; Domenech, S. C.; Lacaze, P. C. *J. Appl. Electrochem.* **2001**, *31*, 49.
16. Herrasti, P.; Kulak, A. N.; Bavykin, D. V.; d. Léon, C. P.; Zekonyteand, J.; Walsh, F. C. *Electrochim. Acta* **2011**, *56*, 1323.
17. Lenz, D. M.; Delamar, M.; Ferreira, C. A. *J. Electroanal. Chem.* **2003**, *540*, 35.
18. Ryu, H.; Sheng, N.; Ohtsuka, T.; Fujita, S.; Kajiyama, H. *Corrosion Sci.* **2012**, *56*, 67.
19. Qi, K.; Qiu, Y.; Chen, Z.; Guo, X. *Corrosion Sci.* **2013**, *69*, 376.
20. Hasanov, R.; Bilgiç, S.; Gece, G. *J. Solid State Electrochem.* **2011**, *15*, 1063.
21. Guo, Z.; Shin, K.; Karki, A. B.; Young, D. P.; Kaner, R. B.; Hahn, H. T. *J. Nanopart Res.* **2009**, *11*, 1441.
22. Yeh, J.-M.; Chang, K. C. *J. Indust. Eng. Chem.* **2008**, *14*, 275.
23. Gao, H.; Xiao, F.; Ching, C. B.; Duan, H. *Appl. Mater. Interfaces* **2011**, *3*, 3049.
24. Hoang, H. V. *Faculty of Natural Science*, Chemnitz University of Technology: Chemnitz, **2007**, p 79.

25. Shiand, J. J.; Zhu, J. *J. Electrochim. Acta* **2011**, *56*, 6008.
26. Chaudhari, S.; Patil, P. P.; Mandale, A. B.; P. K. R. *J. Appl. Polym. Sci.* **2006**, *106*, 220.
27. Liu, Y.-C.; Peng, H. H. 207th Meeting of The Electrochemical Society, Quebec City, Canada, 2005.
28. Jing, Y.; Yongfang, L. *Chinese J. Polym. Sci.* **1996**, *14*, 270.
29. Leeand, J. M.; Lim, K. H. *J. Indust. Eng. Chem.* **2000**, *6*, 157.
30. Omastova, M.; Trchova, M.; Kovarova, J.; Stejskal, J. *Synth. Met.* **2003**, *138*, 447.
31. Tuken, T. *Surf. Coat. Technol.* **2006**, *200*, 4713.
32. Dejeu, J.; Taouil, A. E.; Rougeot, P.; Lakard, S.; Lallemand, F.; Lakard, B. *Synth. Met.* **2010**, *160*, 2540.
33. Ashassi-Sorkhabi, H.; Bagheri, R. *Adv. Polym. Technol.* **2014**, *33*, 3.
34. Pillalamarri, S. K.; Blum, F. D.; Bertino, M. F. *Am. Chem. Soc. Polym. Prepr.* **2005**, *46*, 483.
35. Park, J.-E.; Atobe, M.; Fuchigami, T. *Electrochim. Acta* **2005**, *51*, 849.
36. Spain, E.; Keyes, T. E.; Forster, R. *J. Electrochim. Acta* 20103, 109, 102.
37. Chena, W.; Li, C. M.; Chen, P.; Sun, C. Q. *Electrochim. Acta* **2007**, *52*, 2845.
38. Selvan, S. T.; Hayakawa, T.; Nogami, M.; Mo1ller, M. *J. Phys. Chem. B.* **1999**, *103*, 7441.
39. Elangovan, K.; Sathiya Narayanan, C. *Int. J. Eng. Sci. Technol.* **2010**, *2*, 300.
40. Farzaneh, A.; Ehteshamzadeh, M.; Mohammadi, M. *J. Appl. Electrochem.* **2010**, *41*, 19.
41. Ma, Y.; Hu, H.; Northwood, D.; Nie, X. *J. Mater. Proc. Technol.* **2007**, *182*, 58.
42. Sahoo, P. *Mater. Des.* **2009**, *30*, 1341.
43. Zamanzade, M.; Shahrabi, T.; Gharacheh, E. A. *Mater. Corrosion* **2007**, *58*, 710.
44. Radhakrishnan, S.; Siju, C.; Mahanta, D.; Patil, S.; Madras, G. *Electrochem. Acta* **2009**, *54*, 1249.
45. Ashassi-Sorkhabi, H.; Eshaghi, M. *Corrosion Sci.* **2013**, *77*, 185.
46. Macdonald, J. R. Impedance Spectroscopy Theory, Experiment, and Applications; Wiley: New York, **2005**.
47. Ashassi-Sorkhabi, H.; Ghalebsaz-Jeddi, N. *Ultrasonics Sonochem.* **2006**, *13*, 180.